Journal of Radiation Research, Vol. 61, No. 1, 2020, pp. 1–13
doi: 10.1093/jrr/rrz080
Advance Access Publication: 17 December 2019

Oxidation resistance 1 prevents genome instability through maintenance of G2/M arrest in gamma-ray-irradiated cells

Ako Matsui[1], Junya Kobayashi[2], Shin-ichiro Kanno[3], Kazunari Hashiguchi[1,4], Masahiro Miyaji[1], Yukihiro Yoshikawa[1], Akira Yasui[3] and Qiu-Mei Zhang-Akiyama[1,*]

[1]Laboratory of Stress Response Biology, Department of Zoology, Division of Biological Sciences, Graduate School of Science, Kyoto University, Kitashirakawa-Oiwakecho, Sakyo-ku, Kyoto 606-8502, Japan
[2]Department of Genome Dynamics, Radiation Biology Center, Graduate School of Biostudies, Kyoto University, Yoshidakonoe-cho, Sakyo-ku, Kyoto 606-8501, Japan
[3]Division of Dynamic Proteome in Cancer and Aging, Institute of Development, Aging and Cancer, Tohoku University, 4-1 Seiryocho, Aobaku, Sendai 980-8575, Japan
[4]Department of Biochemistry, Fukuoka Dental College, 2-15-1 Tamura, Sawara-ku, Fukuoka 814-0193, Japan
*Corresponding author. Laboratory of Stress Response Biology, Department of Zoology, Division of Biological Sciences, Graduate School of Science, Kyoto University, Kitashirakawa-Oiwakecho, Sakyo-ku, Kyoto 606-8502, Japan. Tel: +81-75-753-4087; Fax: +81-75-753-4087; Email: qmzhang@kingyo.zool.kyoto-u.ac.jp
(Received 20 April 2019; revised 18 September 2019; editorial decision 18 October 2019)

ABSTRACT

Human oxidation resistance 1 (OXR1) was identified as a protein that decreases genomic mutations in *Escherichia coli* caused by oxidative DNA damage. However, the mechanism by which OXR1 defends against genome instability has not been elucidated. To clarify how OXR1 maintains genome stability, the effects of OXR1-depletion on genome stability were investigated in OXR1-depleted HeLa cells using gamma-rays (γ-rays). The OXR1-depleted cells had higher levels of superoxide and micronucleus (MN) formation than control cells after irradiation. OXR1-overexpression alleviated the increases in reactive oxygen species (ROS) level and MN formation after irradiation. The increased MN formation in irradiated OXR1-depleted cells was partially attenuated by the ROS inhibitor *N*-acetyl-L-cysteine, suggesting that OXR1-depeletion increases ROS-dependent genome instability. We also found that OXR1-depletion shortened the duration of γ-ray-induced G2/M arrest. In the presence of the cell cycle checkpoint inhibitor caffeine, the level of MN formed after irradiation was similar between control and OXR1-depleted cells, demonstrating that OXR1-depletion accelerates MN formation through abrogation of G2/M arrest. In OXR1-depleted cells, the level of cyclin D1 protein expression was increased. Here we report that OXR1 prevents genome instability by cell cycle regulation as well as oxidative stress defense.

Keywords: OXR1; genome stability; oxidative stress; radiation; cell cycle arrest

INTRODUCTION

Reactive oxygen species (ROS), such as superoxide and hydrogen peroxide (H_2O_2), are continuously generated in cells endogenously and exogenously [1]. Under oxidative stress conditions, excessive ROS can damage DNA and accelerate genome instability [1, 2], which may result in tumorigenesis and neurodegenerative disorders [2]. Thus, oxidative stress defense plays an essential role in living organisms.

Oxidation resistance 1 (OXR1) is a gene highly conserved among eukaryotes. It has been reported that OXR1 maintains the normal life span in *Caenorhabditis elegans* [3], prevents neurodegenerative disorders in mice [4, 5] and alleviates other pathological features such as inflammation in nephritis in mice [6]. In many organisms, such as yeast [7, 8], mosquito [9], silkworm [10], worms [3] and mammalian cells [4, 11–15], the depletion or deletion of OXR1 increases the sensitivity

© The Author(s) 2019. Published by Oxford University Press on behalf of The Japanese Radiation Research Society and Japanese Society for Radiation Oncology.
This is an Open Access article distributed under the terms of the Creative Commons Attribution Non-Commercial License (http://creativecommons.org/licenses/by-nc/4.0/), which permits non-commercial re-use, distribution, and reproduction in any medium, provided the original work is properly cited. For commercial re-use, please contact journals.permissions@oup.com

to oxidative stress. This suggests that OXR1 is essential to defend against oxidative stress.

There are several reports that OXR1 maintains genome integrity. In mouse neuronal cells, OXR1-deletion accelerates the formation of 8-oxoG, a major product of oxidative DNA damage [4]. In human cells, OXR1-depletion increases H_2O_2-induced mitochondrial DNA damage [11]. Ectopic expression of human or worm OXR1 suppresses spontaneous mutations in *Escherichia coli* mutants, which lack the genes for repairing oxidative DNA damage [3, 7, 16]. These findings suggest that OXR1 prevents the formation of oxidative DNA damage to protect nuclear and mitochondrial genome integrity. However, the mechanism remains unclear.

Suppression of OXR1 protein decreases transcriptional expression of some ROS detoxification enzymes [4, 9, 11, 12, 15, 17], suggesting that OXR1 is a regulator of the ROS-detoxification system. Moreover, Yang *et al.* previously reported that OXR1-depletion in human cells also affects the transcriptional expression of cell cycle regulators under H_2O_2 treatment conditions [12]. Cell cycle regulation, such as cell cycle checkpoints, is important for maintenance of genome stability [18]. Therefore, it is possible that OXR1 maintains genome stability by regulating the cell cycle. However, this hypothesis has not been confirmed.

To clarify how OXR1 maintains genome stability in human cells, we established an OXR1-depleted HeLa cell line and investigated the effects of OXR1-depletion in cells treated with H_2O_2 or gamma-ray (γ-ray), oxidative stress inducers [19]. Our study demonstrated that OXR1-depletion increases the oxidative stress level and chromosomal instability in irradiated cells. Moreover, we found that OXR1 helps cells maintain genome stability through regulation of the duration of G2/M arrest.

MATERIALS AND METHODS

Construction of plasmids

The coding region of human OXR1 (Protein ID: AAH32710) (Supplementary Fig. S1a, lane 2, see online supplementary material) was amplified by PCR from HeLa first-strand cDNA using the following primer sets: 5′-ATGCTCGAGATGTCTTTTCAGAAACCTAAAGGGACT-3′ and 5′-ATGCGGCCGCTTATTCAAAAGCCCAGATTTCAATATCT-3′. For construction of the glutathione S-trabsferase (GST)-tagged OXR1 expression plasmid (pGEX-OXR1), the OXR1 cDNA fragment was excised by digestion with *Xho*I and *Not*I, and the purified fragment was cloned into the *Sal*I-*Not*I site of the pGEX4T-3 vector (GE Healthcare). FLAG-HA tagged OXR1 expression plasmid vector was constructed as described in a previous report [20]. The pcDNA5/FRT/FH/N-1 vector was originally purchased from Invitrogen as pcDNA5/FRT and modified a cloning site for the expression of FLAG-HA-tagged protein. The OXR1 cDNA fragment was excised by digestion with *Xho*I and *Not*I, and the purified fragment was cloned into an *Xho*I-*Not*I site of pcDNA5/FRT/FHN-1 to generate FLAG-HA-tagged OXR1. For the OXR1 knockdown plasmid, the OXR1 short hairpin RNA-expressing construct (psiRNA-OXR1) was designed to target 1006–1020 in the OXR1 coding sequence (CCDS56548.1) (Supplementary Fig. S1a, lane 1, see online supplementary material). Insert DNA was cloned into the Acc65I-HindIII site of psiRNA-h7SKzeo G1 following the manufacturer's protocol (InvivoGen). The sequence of the hairpin insert was 5′-GTACCTCGGAAGATCAGATTGCAGATAATCAAGAGTTATCTGCAATCTGATCTTCCTTTTTGGAAA-3′.

Protein purification and antibody production

For preparation of recombinant GST-tagged OXR1, *E. coli* BL21 (DE3) were transformed with the pGEX-OXR1 plasmid vector. GST-OXR1 protein expression was induced by the addition of 0.1 mM isopropyl-1-thio-galactopyranoside. GST-OXR1 was purified with a glutathione-sepharose 4B column (GE Healthcare) and then the GST-tag was removed with thrombin. Antiserum was prepared by immunizing rabbits with the purified OXR1 protein (Keari Inc., Japan). Affinity purification was carried out by binding to the purified OXR1 protein. Details are described in the online supplementary material.

Cell culture and treatment

Cells were cultured in Dulbecco's modified Eagle's medium (low glucose, Wako Pure Chemical Industries) supplemented with 10% fetal bovine serum. Cells were maintained at 37°C in a humidified incubator supplied with 5% CO_2. Irradiation with γ-rays was performed using a Cs-137 Gammacell 40 Exactor (NORDION, Canada) at a dose rate of 0.7–0.9 Gy/min, hydrogen peroxide (H_2O_2) (Wako Pure Chemical Industries) diluted with phosphate buffered saline (PBS), 1 M *N*-acetyl-L-cysteine (NAC) (Nacalai Tesque) diluted in distilled water or 100 mM caffeine (Wako Pure Chemical Industries) diluted in PBS under their respective conditions. Details of the treatment conditions are described in the results or figure legends.

Establishment of the human OXR1-depleted and -overexpressed cell lines

HeLa cells were transfected with psiRNA-h7SKz-Luc plasmid (InvivoGen) or psiRNA-OXR1 plasmid using FuGENE HD (Promega) following the manufacturer's protocol. Zeocin (InvivoGen) (200 μg/ml) resistant cells were selected. For site-specific transgene expression, pcDNA5/FRT OXR1 expression vector or empty vector was co-transfected with pOG44 into the Flp-In HEK293 cell lines, respectively, which contained ferritin-like protein recombination target (FRT) sites (Zeocin resistance). Stable clonal integrates were selected with hygromycin. The endogenous OXR1 protein level in whole cells was analyzed by immunoblotting as described in the supplementary methods, see online supplementary material.

Colony formation

An appropriate number of cells was seeded on 60-mm diameter dishes and incubated for 5–6 h following irradiation. After incubation for 10–14 days, the samples were stained with crystal violet in 20% methanol. The number of colonies containing >50 cells was counted.

Detection of the level of intracellular H_2O_2 accumulation

Cells were transfected with the pC1-Hyper-3 plasmid vector (addgene, #42131). After the 24-h incubation, the cells were treated with PBS/50 μM H_2O_2 and simultaneously observed using a BZ-X700 (KEYENCE) inverted microscope. Images were acquired every 15 s at 525–575 nm. The ratio was calculated by fluorescence intensity at 395–415 nm/490–510 nm (F405/F500). Image analysis was performed

with a BZ-X Analyzer. The detailed procedure is described in the online supplementary material.

NADPH detection

Cells were cultured in 60-mm diameter dishes until 80% confluency and treated with 200 μM H_2O_2 for 2 h. The cells were trypsinized, suspended in lysis buffer (50 mM HEPES pH 7.5/10% sucrose/0.1% Triton X-100) and incubated for 10 min on ice. The cells were sonicated and centrifuged at 4°C for 15 min at 13 900 rpm. The absorbance of the supernatant was measured with a UV-1700 PharmaSpec (SHIMADZU) at 340 nm. Change in the NADPH level was calculated by dividing the NADPH level with treatment by that without treatment.

Measurement of the intracellular superoxide level

Cells were seeded on 60-mm diameter dishes and incubated for 1 day to 60–70% confluency. Cells were treated as described in the figure legends, and superoxide was detected using the Total ROS/Superoxide detection kit (ENZ-51010, Enzo Life Sciences) according to the manufacturer's instructions [21] (http://www.enzolifesciences.com/fileadmin/files/manual/ENZ-51010_insert.pdf). Fluorescence intensity for the probe was measured by FACSCaliber using the FL3 (emission: 670 nm LP (long pass)) fluorescence collection lens (BD Biosciences). The data were analyzed using CellQuest Pro Software (BD Biosciences). See BD Biosciences, 2007 [22] (https://www.bdbiosciences.com/documents/BD_FACSCalibur_instructions.pdf) for details.

Fluorescence microscopy

Fluorescence images were taken by fluorescence microscopy with an OLYMPUS IX70 equipped with an OLYMPUS DP50 using the 10× or 20× objective lens.

Quantification of the intracellular ROS level

Cells were incubated for 22 h after irradiation. The cells were washed with PBS and treated with 10 μM chloromethyl derivative of 2', 7'-dichlorodihydrofluorescein diacetate (CM-H_2DCFDA) (C6827, Invitrogen, in serum-free medium at 37°C for 30 min. The cells were washed with PBS and the fluorescence of DCF was observed with the fluorescence microscope equipped with a 10× objective. Images were analyzed by Fiji software (http://fiji.sc) [23] to measure fluorescence intensity.

Cellular ATP

Intracellular ATP was detected by ATP assay reagent (CA50 TOYO B-Net). Cells were irradiated and incubated for 20 h. The cells were trypsinized, and then 5x 10^3 cells/100 μL of DMEM/10% FBS were transferred into 96-well white-bottom plate. The cells were mixed with 100 μL of ATP assay reagent by tuple mixer (TWIN3–28 IWAKI) for 1 min and incubated at 23°C for 30 min. Chemiluminescence was measured by Centro LB 960 Microplate Luminometer (Berthold Technologies).

Cell synchronization

For G1/S-synchronizing experiments, the thymidine/hydroxyurea or double-thymidine method was used. OXR1-depleted HeLa cells were seeded in culture dishes and cultured for 2 days. The cells were treated with 2.5 mM thymidine (Wako Pure Chemical Industries) for 20–24 h. The cells were incubated in fresh medium for 10 h, and then hydroxyurea (Acros Organics) was added to a final concentration of 1 mM. After 14–16 h, the cells were treated with the indicated reagents. OXR1-overexpressing HEK293 cells were treated with 2 mM thymidine for 16 h. At 9 h after thymidine treatment, the cells were again exposed to 2 mM thymidine for 16 h.

Measurement of micronucleus frequency

Cells were seeded on 35-mm diameter culture dishes and cultured for 1–2 days. The cells were synchronized at G1/S phase and then exposed to radiation or H_2O_2. After 22–24 h, the cells were fixed with PBS/4% paraformaldehyde for 15 min at 4°C and permeabilized with 0.1% Triton X-100 for 5 min at room temperature. Nuclei were stained with 5 μg/ml of 4′,6-diamidino-2-phenylindole, dihydrochloride (DAPI, Nacalai Tesque) for 5 min. The cells were washed three times with PBS. Fluorescence microscopy images were taken using the 10× or 20× objective lens. The percentage of cells with micronuclei was calculated (300–4400 cells per condition per experiment).

Cell cycle

Cells were seeded on 60-mm diameter culture dishes and cultured to ∼40% confluency for 1 day. The cells were synchronized at G1/S phase followed by irradiation. The cells were harvested by trypsinization and then washed with PBS. The cells were fixed with 70% ethanol at −20°C overnight. The cells were centrifuged and resuspended in PBS containing 5 μg/ml of RNase, and then counter-stained with 50 μg/ml of propidium iodide (Sigma-Aldrich). The suspension was then analyzed using FACSCaliber (BD Biosciences) to create DNA content frequency histograms for 20 000 cells per sample. The cell cycle profiles were prepared using the BD CellQuest Pro Software (BD Biosciences).

Immunoblotting

Cultured cells were exposed to γ-rays and incubated for the indicated time. Cellular pellets were lysed in ice-cold TNE buffer (50 mM Tris-HCl pH 7.5/100 mM NaCl/1 mM EDTA pH 8.0/50 mM NaF/12 mM $Na_4P_2O_7$/1 mM Na_3VO_4/1% Triton X-100/1 mM phenylmethylsulfonyl fluoride/10 ng/ml of leupeptin) for 15 min on ice. The protein concentrations of supernatants were measured using the BCA Protein Assay Kit (Pierce). 5x SDS loading buffer was added to these samples and they were subjected to SDS polyacrylamide gel electrophoresis (SDS-PAGE). Proteins were transferred to nitrocellulose membranes and then blocked with 3% bovine serum albumin (BSA) or 5% non-fat milk in PBST (PBS/0.05% Tween 20) for 1 h at room temperature. Membranes were incubated for 1 h at room temperature or overnight at 4°C with primary antibodies, and then reacted with horseradish peroxidase (HRP)-conjugated secondary antibodies for 1 h at room temperature. The membranes were washed with PBST after incubation with each antibody. Bound antibodies were visualized by chemiluminescence (ECL; Amersham or SuperSignal West Pico Chemiluminescent; Thermo fisher scientific). Membranes were exposed to X-ray film (FUJIFILM). Images were analyzed by ImageJ 1.5a (Wayne Rasband National Institute of Health, USA http://imagej.nih.gov/ij). Antibodies used were: OXR1 (purification in this study, 1:4000, Fig. 1g was obtained using A302-035A-T, BETHYL, 1:2,000), MK2 (#3042,

Cell Signaling Technology, 1:1000), cyclin D1 (sc-753, Santa Cruz Biotechnology, 1:500), beta-tubulin (sc-9104, Santa Cruz Biotechnology, 1:3000), beta-actin (A5361, Sigma-Aldrich, 1:10000), rabbit-IgG-HRP (sc-2030, Santa Cruz Biotechnology, 1:5000), mouse-IgG-HRP (sc-2005, Santa Cruz Biotechnology, 1:5000). The detection of OXR1 protein in whole cell samples was performed as described in the online supplementary material.

Immunoprecipitation and anoLiquid Chromatography-Mass spectrometry (nanoLC/MS/MS)

The cell line induced to express FLAG-OXR1 by the Flp-In T-REx system and the control cell line with the pcDNA5/FRT/TO vector only were established as described in the online supplementary material. Proteomic analysis was performed as previously reported [24]. The cells were suspended in 1 mL of extraction buffer (50 mM HEPES pH 7.4/300 mM NaCl/0.2% NP-40) and sonicated. The cell lysates were clarified by centrifugation at 12 000 rpm for 30 min at 4°C. The supernatants were filtered using a Minisart Syringe Filter (Sartorius) and incubated with anti-FLAG M2 antibody beads (40 μL, Sigma-Aldrich) for 4 h in the presence of benzonase nuclease (10 μg/ml, Millipore) at 4°C. After washing three times with washing buffer (50 mM HEPES pH 7.4/150 mM NaCl/0.1% NP-40) and once with PBS, the bound proteins were eluted with 40 μL of 0.1 M glycine buffer at pH 3.0. The eluted samples were neutralized by 4 μL of 1 M Tris-HCl buffer at pH 9.5 and suspended in SDS-PAGE sample buffer. The samples were boiled for 5 min and resolved by SDS-PAGE. The gel was stained using a Wako Mass silver stain kit. Gel slippage was reduced by 100 mM of dithiothreitol (DTT) and alkylated by 100 mM iodoacetamide. After washing, the gels were incubated with trypsin overnight at 30°C. Recovered peptides were desalted by Ziptip c18 (Millipore). Samples were analyzed by a nanoLC/MS/MS system (DiNa HPLC system KYA TECH Corporation/QSTAR XL Applied Biosystems). Mass data acquisitions were piloted by Mascot software.

Statistical analysis

The data for the statistical assay comprised more than three independent experiments with technical triplicates. Pairwise comparison between control cells and mutant cells was performed by ANOVA with Welch's or Student's t-test. Multiple comparisons were conducted by ANOVA with the Tukey-Kramer or Dunnett's test. Data were analyzed using R 3.5.0 GUI 1.70 El Capitan build (7521), S. Urbanek, H.-J. Bibiko and Stefano M. Iacus, see http://www.R-project.org for more information. *P*-values < 0.05 were considered significant. Data are expressed as the mean ± s.e.m. or s.d.

Data availability

The datasets generated or analyzed during this study are included in this article (and in the online supplementary material).

RESULTS

Stable knockdown of OXR1 accelerated oxidative stress after H_2O_2 treatment or γ-ray irradiation in HeLa cells

To establish an OXR1-depleted human cell line, we designed an OXR1 short hairpin RNA (shOXR1)-expressing-plasmid vector for targeted depletion of OXR1 (psiRNA-OXR1) (Supplementary Fig. S1a, lane 1, see online supplementary material). shOXR1 targets exon 8 in the OXR1 coding sequence, which is included in almost all isoforms of OXR1 except for isoforms 5 (Supplementary Fig. S1a, lane 3, see online supplementary material) and 6. HeLa cells were transfected with psiRNA-OXR1, and an OXR1-depleted cell line was isolated. In this cell line, the expression level of OXR1 was examined by immunoblotting with anti-OXR1 antibody, which recognizes both the long and short isoforms of purified OXR1 protein at 112 and 28 kDa, respectively (Supplementary Fig. S1b and c, see online supplementary material). The 112 kDa protein was detected in the cellular extract of the control cell line transfected with Luciferase short hairpin RNA (shLuci)-expressing plasmid vector, but the 28 kDa protein was not. These results suggest that the long isoform of OXR1 is mainly expressed in HeLa cells, whereas expression of the short isoform is minimal. The cloned OXR1-depleted cell line exhibited a 90% reduction in the long isoform (Fig. 1a), which was similar to the result obtained by another type of anti-OXR1 antibody (Supplementary Fig. S1d, see online supplementary material). These results indicated that the OXR1-depleted HeLa cell line was successfully established. Additionally, control cells and OXR1-depleted cells showed sensitivity to 0.25 mM H_2O_2 in the ratio of 27.7% (±4.81) and 13.1% (±8.61), respectively (Supplementary Fig. S1e, see online supplementary material), confirming that the established OXR1-depleted cells were more sensitive to H_2O_2 than control cells, as previously reported [4, 11, 12, 15]. Sensitivity in OXR1-depleted cells was not detected after γ-ray irradiation, suggesting that the role of OXR1 in irradiated cells is different from that in H_2O_2-treated cells (Fig. 1b). OXR1-depleted cells were not more sensitive to treatment with the superoxide generator, pyocyanin [25] (Supplementary Fig. S1f, see online supplementary material), which was similar to the results previously reported [11].

To investigate whether OXR1-depletion accelerates H_2O_2 accumulation, cells were exposed to H_2O_2, and the H_2O_2 level in living cells was monitored [26], as described in detail in the supplementary methods section, see online supplementary material. No significant difference was found between control cells and OXR1-depleted cells (Fig. 1c). This result suggests that OXR1-depletion does not impair the intracellular H_2O_2-detoxification system. As NADPH is consumed for ROS-detoxification, the NADPH level decreases under oxidative stress conditions [27]. Cells were exposed to H_2O_2 for 2 h, and the fluctuation in NADPH level, defined as the NADPH level in H_2O_2-treated cells divided by that in non-treated cells, was calculated. OXR1-depletion reduced the NADPH level significantly (Fig. 1d). This result indicates that OXR1-depletion increases the oxidative stress level in H_2O_2-treated cells. OXR1-overexpression was reported to alleviate the increase in the cytoplasmic superoxide level in mouse neuronal cells under oxidative stress conditions [13, 28]. To examine whether OXR1-depletion also affects the intracellular superoxide level, OXR1-depleted cells were treated with H_2O_2 for 2 h and the total cellular superoxide level was measured using a superoxide-reacting fluorescent probe [21]. H_2O_2 treatment increased the superoxide level in OXR1-depleted cells, and the level in OXR1-depleted cells was approximately 1.4-fold higher than that in control cells (superoxide level (±s.e.m.): shLuci (luciferase), 0.76 (0.02); shOXR1, 1.05 (0.06)) (Fig. 1e, right panel). Similar results were confirmed 4 h after irradiation with 10 Gy of γ-rays (superoxide level (±s.e.m.): shLuci, 1.01 (0.04); shOXR1, 1.64 (0.16)) (Fig. 1f). These results suggest that OXR1-depletion enhances

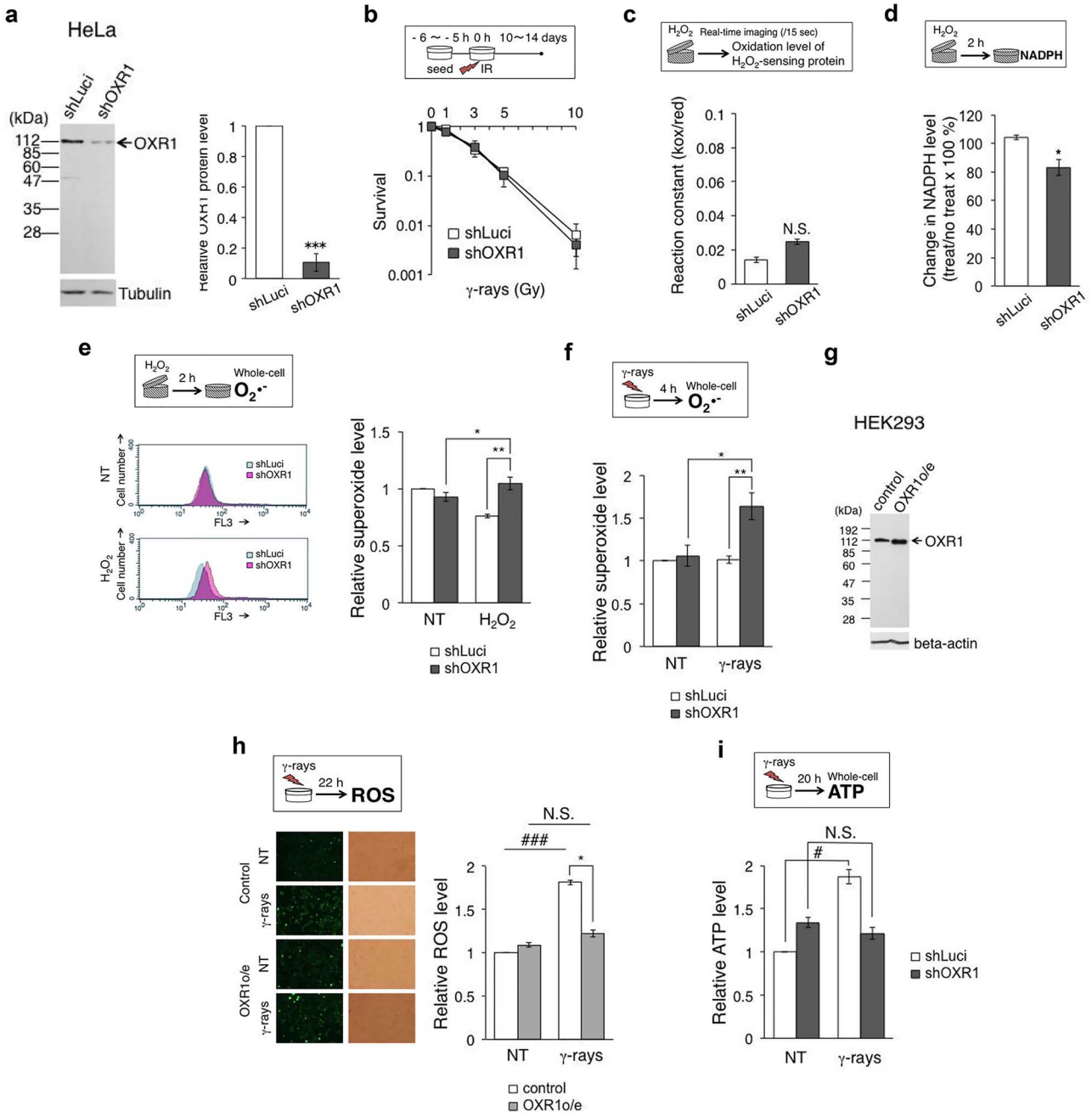

Fig. 1. OXR1-depletion increases the superoxide level after irradiation or H_2O_2 treatment. (a) HeLa cells were transfected with psiRNA-OXR1 or psiRNA-luciferase, and a stably OXR1-depleted cell line (shOXR1) or control cell line (shLuci) was cloned. Left, representative Western blot of OXR1 protein expression in the shOXR1 or control cell line (shLuci). Right, quantification of the OXR1 protein expression level. Mean ± s.e.m. of *n* = four independent experiments, $^{***}P < 0.001$, two-tailed Welch's t-test. (b) Quantification of cellular sensitivity after irradiation with γ-rays. OXR1-depleted HeLa cells (shOXR1) and control cells (shLuci) were irradiated with 1–10 Gy of γ-rays (0.7 Gy/min). Mean ± s.d. of *n* = three independent experiments. (c) Quantification of the accumulation of H_2O_2 in cells exposed to 50 μM H_2O_2 by monitoring after the addition of H_2O_2. Mean ± s.e.m. of *n* = three independent experiments, two-tailed Student's t-test; N.S., not significant. (d) Quantification of the change in the NADPH level after treatment with 200 μM H_2O_2 for 2 h. Mean ± s.e.m. of *n* = three independent experiments, $^{*}P < 0.05$, two-tailed Student's t-test. (e) The superoxide level was quantified after treatment with 100 μM H_2O_2 for 2 h (*n* = three independent experiments). Left, representative histograms indicating the superoxide level in cells treated with H_2O_2. Right, quantification of the superoxide level.

superoxide-derived oxidative stress after H_2O_2 treatment and γ-ray irradiation. After pyocyanin treatment, superoxide level increased in both OXR1-depleted cells and control cells. The increase was not accelerated by OXR1-depletion as long as it was investigated (Supplementary Fig. S2, see online supplementary material). To confirm that OXR1 inhibits irradiation-induced oxidative stress, an OXR1-overexpressing HEK293 cell line was established (Fig. 1g), and the ROS level in the cell line was measured by CM-H_2DCFDA after irradiation with γ-rays (Fig. 1h, left panel). The used OXR1 has been reported to decrease mutation frequency in an E. coli mutMmutY and mutT mutant. After irradiation, ROS level increased in control HEK293 cells, whereas an increase in ROS level was not found in OXR1-overexpressing cells (Fig. 1h, right panel). These results indicate that OXR1 prevented irradiation-induced oxidative stress. The alteration of mitochondrial functions causes the change in intracellular ATP level [29]. It has been demonstrated that functional mitochondria increase the ATP level in cancer cell lines by 24 h after irradiation [30, 31]. To investigate whether OXR1-depletion affects mitochondrial functions after irradiation, ATP level was measured. In control cells, ATP level was increased by γ-ray irradiation (Fig. 1i). On the other hand, the increase was not found in OXR1-depleted cells. Our results suggest that OXR1 contributes to maintenance of mitochondrial functions in irradiated cells.

OXR1-depletion increased micronucleus formation in cells exposed to oxidative stress

To investigate whether OXR1-depletion accelerates genome instability in human cells under oxidative stress conditions, OXR1-depleted cells synchronized in G1/S phase were treated with 1 mM H_2O_2 for 0.5 or 1 h, and were then recovered for 24.5 or 24 h, respectively. Next, the percentage of cells with micronuclei (MN), a hallmark of chromosomal instability [32], was measured. OXR1-depleted cells had a higher percentage of cells with MN than control cells after the 1-h H_2O_2 treatment (Fig. 2a). This result suggests that OXR1-depletion increases MN formation under oxidative stress. When cells were irradiated with γ-rays and incubated for 24 h, in control cells, the level of MN formation at 1 or 3 Gy tended to increase compared with non-irradiated cells. After irradiation with 10 Gy, it was reduced to a similar level to that in non-irradiated cells (Fig. 2b). Of note, OXR1-depleted cells had a higher level of MN formation after irradiation with 10 Gy than both non-irradiated cells and control cells. OXR1-overexpressing HEK293 cells showed partial alleviation of the increase in MN formation after irradiation (Fig. 2c), indicating that OXR1 prevented irradiation-induced MN formation. To confirm whether radiation-induced MN formation is accelerated by ROS in OXR1-depleted cells, cells were irradiated in the presence of NAC, an antioxidant to several types of ROS [33, 34]. In this experiment, three NAC treatment conditions were set; conditions 2, 3 and 4 (Fig. 2d, left panel). After irradiation, the first elevation of the intracellular ROS level occurs by at least 0.5 h, which is thought to be caused by ionization of water (radiolysis-derived ROS) [19], and then the elevated ROS level decreases to the non-irradiated level [35]. The ROS level begins to increase again through endogenous ROS production (later-produced ROS) at least 4 h after irradiation, and it is maintained at a high level [30, 35, 36]. Conditions 2 and 3 targeted radiolysis-derived ROS and condition 4 targeted later-produced ROS. In condition 4, in which the cells were treated with 1 mM NAC from 4 h to 22.5 h after irradiation, the percentage of cells with MN in NAC-treated OXR1-depelted cells was significantly decreased compared with NAC-untreated OXR1-depleted cells (Fig. 2d, right panel). This result demonstrated that ROS, especially later-produced ROS, increase MN formation in irradiated OXR1-depleted cells.

OXR1-depletion accelerated MN formation by shortening the duration of G2/M arrest induced after γ-ray irradiation

OXR1 prevents the accumulation of oxidative DNA damage [4]. Oxidative DNA damage can cause DNA-strand breaks, which result in micronucleus formation [2, 32, 37]. To investigate whether γ-ray-induced DNA damage is increased in OXR1-depleted cells, cells were irradiated and recovered for 0, 0.5 or 1 h, and then the amount of DNA strand breaks was measured by the alkaline comet assay [38]. The amount of DNA damage increased just after irradiation in both the control cells and OXR1-depleted cells. The amount was slightly higher in OXR1-depleted cells, although no significant difference was detected between control cells and OXR1-depleted cells (Supplementary Fig. S3a, see online supplementary material). Half an hour after irradiation, the amount of DNA damage decreased to approximately the non-irradiation level in both control cells and OXR1-depleted cells, which was similar to that at 1 and 4 h after irradiation (Supplementary Fig. S3b, see online supplementary material). These results indicated that DNA damage generated just after irradiation was normally repaired in OXR1-depleted cells. This suggested that the increase in MN in

(f) Quantification of the superoxide level in cells irradiated with 10 Gy of γ-rays and incubated for 4 h (*n* = four independent experiments). (e, f) Mean ± s.e.m., $^{*}P < 0.05$, $^{**}P < 0.01$, two-way ANOVA with two-tailed Student's t-test. NT, no treatment. (g) Detection of OXR1 protein expression in established cell line. Protein expression in cellular extract was analyzed by western blotting using anti-OXR1 antibody (A302-035A-T, BETHYL); control, control HEK293 cells. OXR1o/e, OXR1-overexpressing HEK293 cells. (h) Quantification of intracellular ROS level. OXR1-overexpressed and control HEK293 cells were irradiated with 2 Gy of γ-rays and incubated for 22 h. Intracellular ROS were detected with CM-H_2DCFDA. Left, representative images obtained by fluorescence microscopy: left images, fluorescent field; right images, bright field. Right, quantification of ROS level. Mean ± s.e.m. of *n* = four independent experiments, $^{###}P < 0.001$, two-way ANOVA with Dunnett's multiple comparisons test, $^{*}P < 0.05$, two-tailed Student's t-test. N.S., not significant. NT, non-irradiation. (i) Detection of intracellular ATP. 20 h after irradiation with 10 Gy of γ-rays, intracellular ATP was analyzed. Mean ± s.e.m. of *n* = three independent experiments, $^{\#}P < 0.05$, two-way ANOVA with Dunnett's multiple comparisons test. N.S., not significant. NT, non-irradiation.

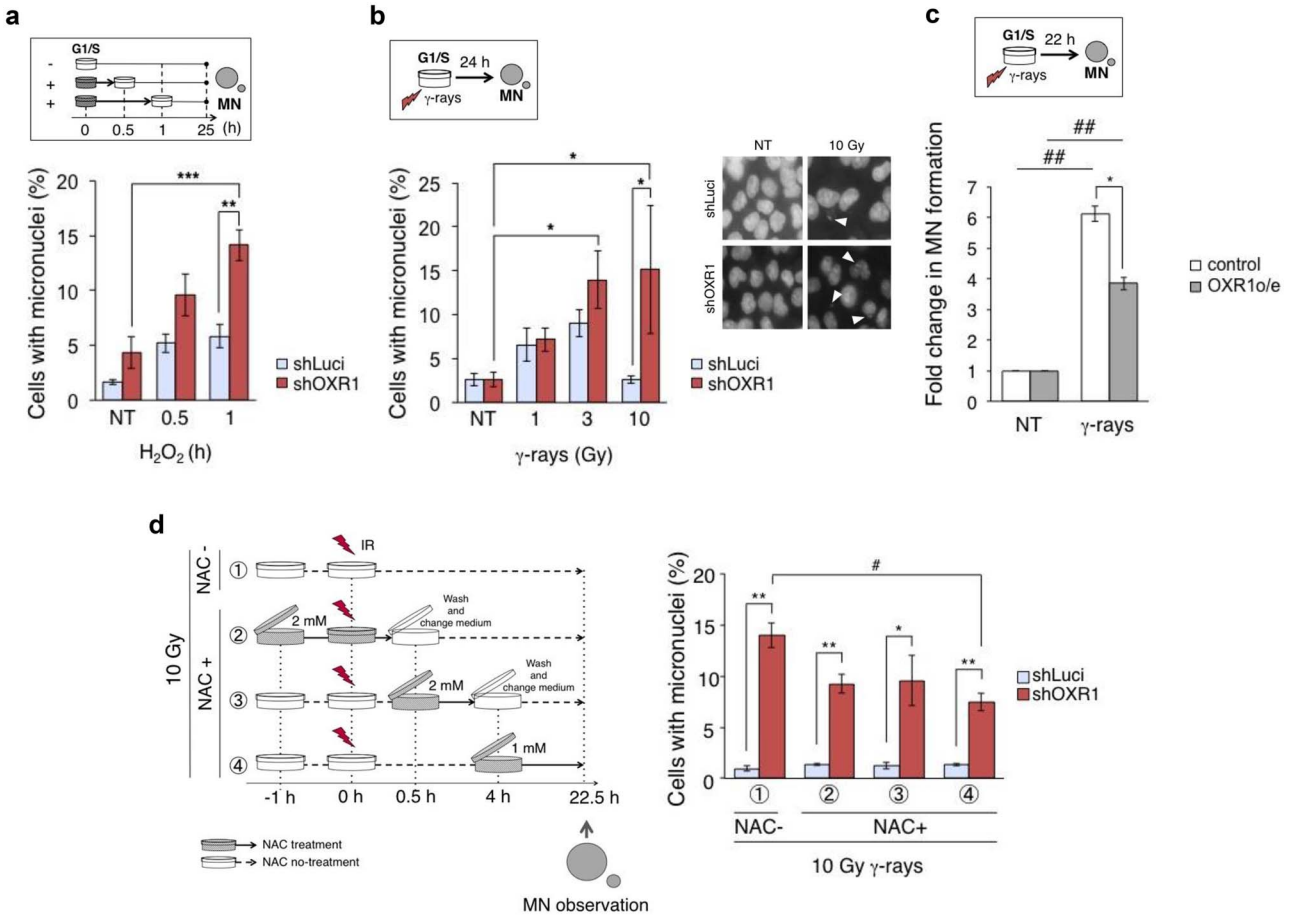

Fig. 2. OXR1-depletion increases micronucleus formation in cells under oxidative stress conditions. **(a, b) Quantification of the percentage of OXR1-depleted HeLa cells (shOXR1) or control cells (shLuci) with micronuclei at the indicated time after treatment (≥ 700 cells were analyzed per condition per experiment). Cells synchronized in G1/S phase were released from arrest and simultaneously treated with (a) 1 mM H_2O_2 for 0.5 (*n* = four independent experiments) or 1 h and (b) 0.5–10 Gy of γ-rays (0.7 Gy/min) (*n* = three independent experiments). (b) Right panels, representative images of DAPI-stained nuclei. Arrowheads indicate micronuclei. Mean ± s.e.m., $^{*}P < 0.05$, $^{**}P < 0.01$, $^{***}P < 0.001$, two-way ANOVA with the Tukey-Kramer multiple comparisons procedure. NT, non-irradiation. (c) Quantification of MN formation in OXR1-overexpressed cells. G1/S-synchronized cells were irradiated, and after 22 h, micronuclei were observed (≥ 1800 cells per condition per experiment). Mean ± s.e.m. of *n* = three independent experiments, $^{\#\#}P < 0.01$, Dunnett's multiple comparisons test, $^{*}P < 0.05$, two-tailed Student's t-test. NT, non-irradiation. OXR1o/e, OXR1-overexpressing. (d) The effects of NAC treatment on micronucleus formation. Cells were treated with 1 or 2 mM NAC-containing medium before or after irradiation with 10 Gy of γ-rays. Left, the scheme of NAC treatment. Right, quantification of the percentage of cells with micronuclei (≥ 1,000 cells per condition per experiment). Mean ± s.e.m. of *n* = four independent experiments, $^{\#}P < 0.05$, two-way ANOVA with Dunnett's multiple comparisons test, $^{*}P < 0.05$, $^{**}P < 0.01$, two-tailed Welch's t-test.**

OXR1-depleted cells was not caused by DNA damage generated just after irradiation.

After irradiation, MN formation can also be increased by overriding cell cycle arrest [32, 39]. As cells were irradiated at G1/S phase in our studies, release from G2/M arrest was needed for MN formation [40]. To investigate the cell cycle profile in irradiated OXR1-depleted cells, G1/S phase-synchronized cells were exposed to 10 Gy of γ-rays, and the change in cell cycle distribution was observed during the 24-h recovery period. In non-irradiated wild type cells (WT), control cells (shLuci) and OXR1-depleted cells (shOXR1), a similar cell cycle profile was observed. After 16- and 24-h culture, almost all of the cells were in G1-phase, and G2- and M-phase cells were rarely detected (Fig. 3a, right panels). This indicated that cell cycle started with G1/S phase and sequentially progressed. Irradiated WT cells and shLuci cells had similar results. In irradiated shLuci cells, the percentage of G2 and M phase-cells was 92.6% after 16 h and 94.0% after 24 h.

These results demonstrate that G2/M arrest is induced by irradiation with 10 Gy of γ-rays and is maintained. Moreover, in irradiated shOXR1 cells, the percentage of G2 and M phase cells increased to 72.0% after 16 h, indicating that G2/M arrest was induced. However, after 24 h, shOXR1 cells in G2 and M phase decreased to 37.7% and G1 phase cells increased to 55.3%. This result demonstrated that OXR1-depleted cells were released from G2/M arrest between 16 and 24 h after irradiation. Similar results were obtained for asynchronous cells (Supplementary Fig. S4, see online supplementary material). Our data suggest that OXR1-depletion shortens the duration of irradiation-induced G2/M arrest. We observed an increase in G2- and M-phase cells 36 h after treatment with 1 mM H_2O_2 for 1 h (Supplementary Fig. S5, see online supplementary material), which is similar to the result reported by Yang *et al.* [12]. This suggests that overriding cell cycle arrest by depletion of OXR1 is specific to irradiated cells. As shown in Fig. 3b, cells were exposed to NAC from 4 h after irradiation. The NAC treatment did not change the percentage of cells in G2 and M phase in OXR1-depleted HeLa cells or control cells, suggesting that the shortened G2/M arrest caused the increase in MN formation in OXR1-depleted cells (Fig. 3b right panels). To confirm that the shorter duration of G2/M arrest by OXR1-depletion increases MN formation, G1/S-synchronized cells were irradiated and incubated in caffeine-containing medium. Caffeine inhibits cell cycle arrest by inactivating DNA damage responses, including the Ataxia telangiectasia and Rad3-related protein (ATR) pathway, triggered by irradiation [41, 42]. As shown in Fig. 3c left panel, under caffeine treatment, almost all of the OXR1-depleted cells and control cells were in G1 phase 24 h after irradiation, indicating that G2/M arrest was shortened or suppressed. In this condition, MN formation increased in OXR1-depleted cells and control cells to a similar extent after irradiation (Fig. 3c right graph), demonstrating that OXR1-depletion increases MN formation thorough shortening the duration of G2/M arrest after irradiation.

OXR1-depletion affects the state of the cell cycle regulator

Activated Mitogen-activated protein kinase-activated protein (MAPKAP) kinase 2 (MK2), phosphorylated MK2 (pMK2), contributes to maintenance of G2/M arrest in response to damaged DNA [43, 44]. MK2-depletion shortens the duration of G2 arrest in DNA-damaged cells [43, 44]. Cyclin D1 is generally known to function in G1 progress [45, 46], whereas it has been reported that cyclin D1-up-regulated cells have a shorter G2/M arrest after irradiation [47]. To confirm the effects of OXR1-depletion on the maintenance of the duration of G2/M arrest at the molecular level, the MK2 phosphorylation state and the expression level of cyclin D1 were examined by immunoblotting (Fig. 4a).

OXR1 expression level was not changed by irradiation (Fig. 4b). One hour after irradiation, MK2 phosphorylation was induced by irradiation (Fig. 4c). Then, 4 and 16 h later, the level of MK2 phosphorylation decreased to a similar level to non-irradiation. No difference between OXR1-depeleted cells and control cells was detected in the change of MK2 phosphorylation under irradiation conditions. As shown in Fig. 4a, the anti-cyclin D1 antibody used detected two bands at ∼37 kDa, as previously reported [48]. We found that the cyclin D1 protein level in OXR1-depleted cells was higher than that in control cells (Fig. 4d), indicating that OXR1-depletion affects the protein expression of cyclin D1 in irradiated cells.

To elucidate the molecular mechanism of cell cycle control of OXR1, OXR1 binding proteins were explored. Of note, the proteins related to cyclin D1 expression, beta-catenin and glycogen synthase kinase-3 (GSK3beta) [49, 50], were detected (Fig. 4e). GSK3beta is activated by the protein phosphatase 1 (PP1) complex [51, 52]. Some PP1 complex proteins, such as PP1 regulatory subunit 9A (PPP1R9A) and 9B (PPP1R9B), and PP1 catalytic subunit alpha (PPP1CA), beta (PPP1CB) and gamma (PPP1CC), were also detected. These results suggest that OXR1 interacts with the regulators of cyclin D1 expression (Supplementary Fig. S6, see online supplementary material).

DISCUSSION

OXR1, which inhibits oxidative stress, is thought to suppress oxidative DNA damage-derived genome instability [3, 7, 16]. However, little is known about the mechanism by which OXR1 protects genome stability. To clarify how OXR1 contributes to the maintenance of genome stability, we established an OXR1-depleted cell line, and found that superoxide level increased in OXR1-depleted cells after irradiation with γ-rays (Fig. 1f). OXR1-depletion accelerated MN formation, which was caused by oxidative stress and shorter duration of G2/M arrest (Figs 2 and 3). OXR1-depleted cells showed an abnormal state of the cell cycle regulator (Fig. 4).

OXR1-depletion caused an increase in the intracellular superoxide level induced by 2 h after continuous treatment with H_2O_2 or 4 h after irradiation with γ-rays in human cells, indicating that OXR1 contributes to inhibition of oxidative stress (Fig. 1e, f). As suggested in previous reports [3], OXR1 may accelerate the elimination of superoxide. NADPH is consumed by superoxide production as well as ROS-detoxification [27]. The result that OXR1-depletion lowered the NADPH level (Fig. 1d) may reflect excessive ROS-detoxification and/or an increase in superoxide production. Previous reports have demonstrated that OXR1 contributes to regulation of mitochondrial genome integrity [11] and mitochondrial morphology [14] under oxidative stress conditions. In the present study, we found that OXR1-depletion inhibited the increase in intracellular ATP level (Fig. 1i), suggesting that mitochondrial functions are abrogated. Mitochondrial dysfunction increases the superoxide level [53]. It is possible that the increased superoxide caused by OXR1 depletion is derived from mitochondria.

Next, we investigated whether OXR1 maintains genome stability through oxidative stress inhibition. MN, which are formed by chromosome mis-segregation [32], are one indicator of genome instability. OXR1-depletion exhibited MN formation after irradiation, and the increased MN formation was mitigated by NAC treatment, suggesting that OXR1 protects genome stability by inhibiting oxidative stress (Fig. 2b and d). Furthermore, the result that NAC treatment was significantly effective in alleviating MN formation 4 h after irradiation suggests that OXR1 protects genome stability through inhibiting the increase in superoxide level. The results that OXR1-overexpression alleviated the irradiation-derived increase in later-produced ROS level (Fig. 1h) and MN formation (Fig. 2c) support this suggestion.

OXR1-depletion increased MN formation through abrogation of G2/M arrest (Fig. 3c). G2/M arrest is induced, and then it is

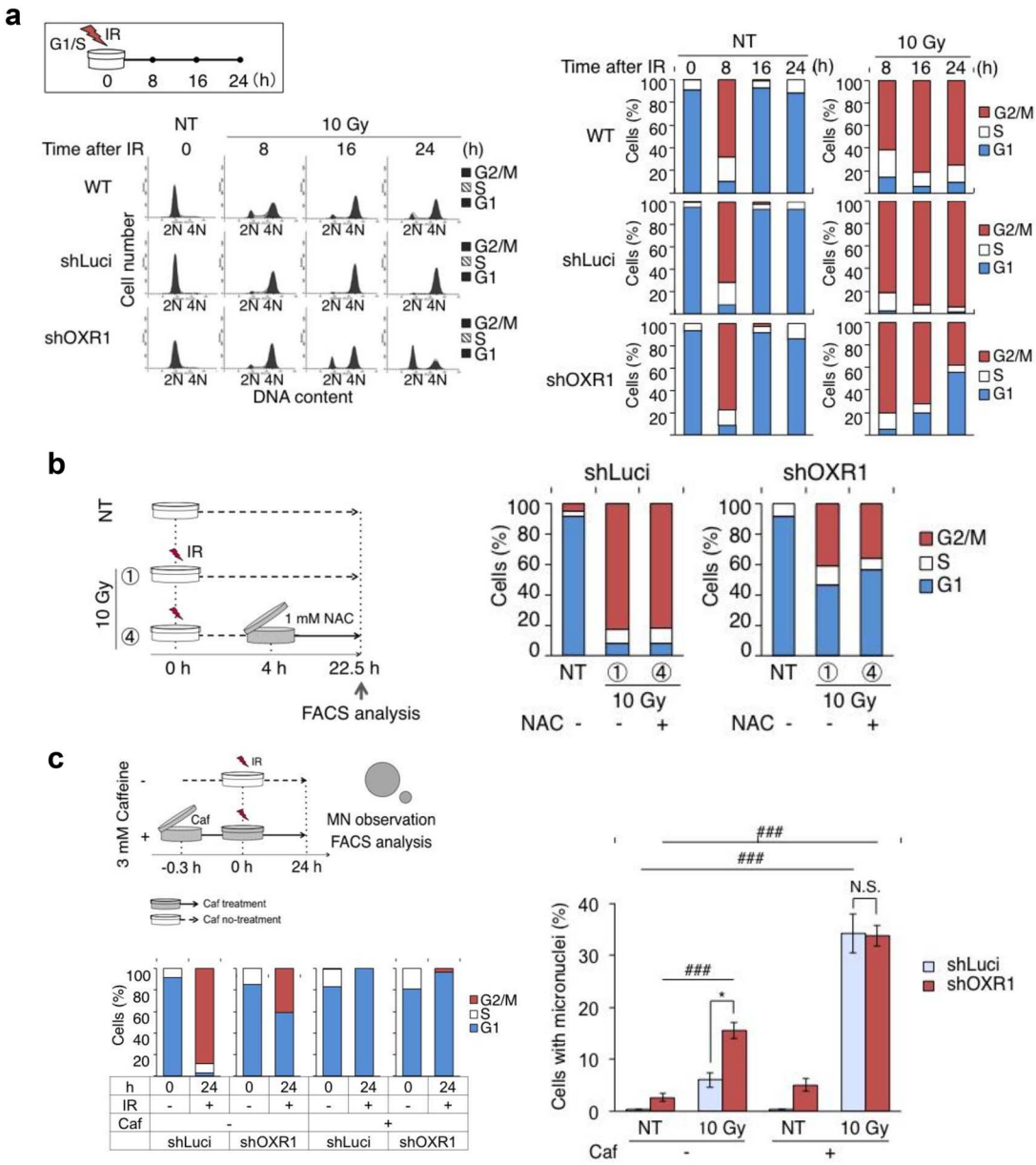

Fig. 3. Shortened G2/M arrest in OXR1-depleted cells increased micronucleus formation after γ-ray irradiation. (a) The cell cycle profile of cells irradiated with 10 Gy of γ-rays. G1/S phase-synchronized OXR1-depleted HeLa cells (shOXR1), control cells (shLuci) and non-transfected wild type cells (WT) were irradiated with 10 Gy of γ-rays (0.9 Gy/min) (IR) and incubated for the indicated time. Left, histograms representing cell cycle distribution. 2 N, 4 N: DNA content (N: nucleotide). Right, bar graphs obtained from left histograms. NT, non-irradiation. (b) The effects of NAC treatment on cell cycle arrest. Cells were irradiated in the presence or absence of 1 mM NAC. Left, the scheme of NAC treatment. Right, quantification of cell cycle distribution. NAC conditions are labeled in the same manner as in Fig. 2d. NT, non-irradiation. (c) The effects of caffeine on micronucleus formation. OXR1-depleted HeLa cells (shOXR1) and control cells (shLuci) were treated with 3 mM caffeine (Caf) for 20 min before irradiation with 10 Gy of γ-rays (IR) and incubated for 24 h in caffeine-containing medium. Left upper panel, the scheme of caffeine treatment. Left bottom panel, cell cycle distribution. h, hours after IR. Right, quantification of micronucleus frequency (≥ 600 cells per condition per experiment). Mean ± s.e.m. of n = three independent experiments, $^{###}P < 0.001$, three-way ANOVA with Dunnett's multiple comparisons test, $^{*}P < 0.05$, two-tailed Welch's t-test and Student's t-test. N.S., not significant. NT, non-irradiation.

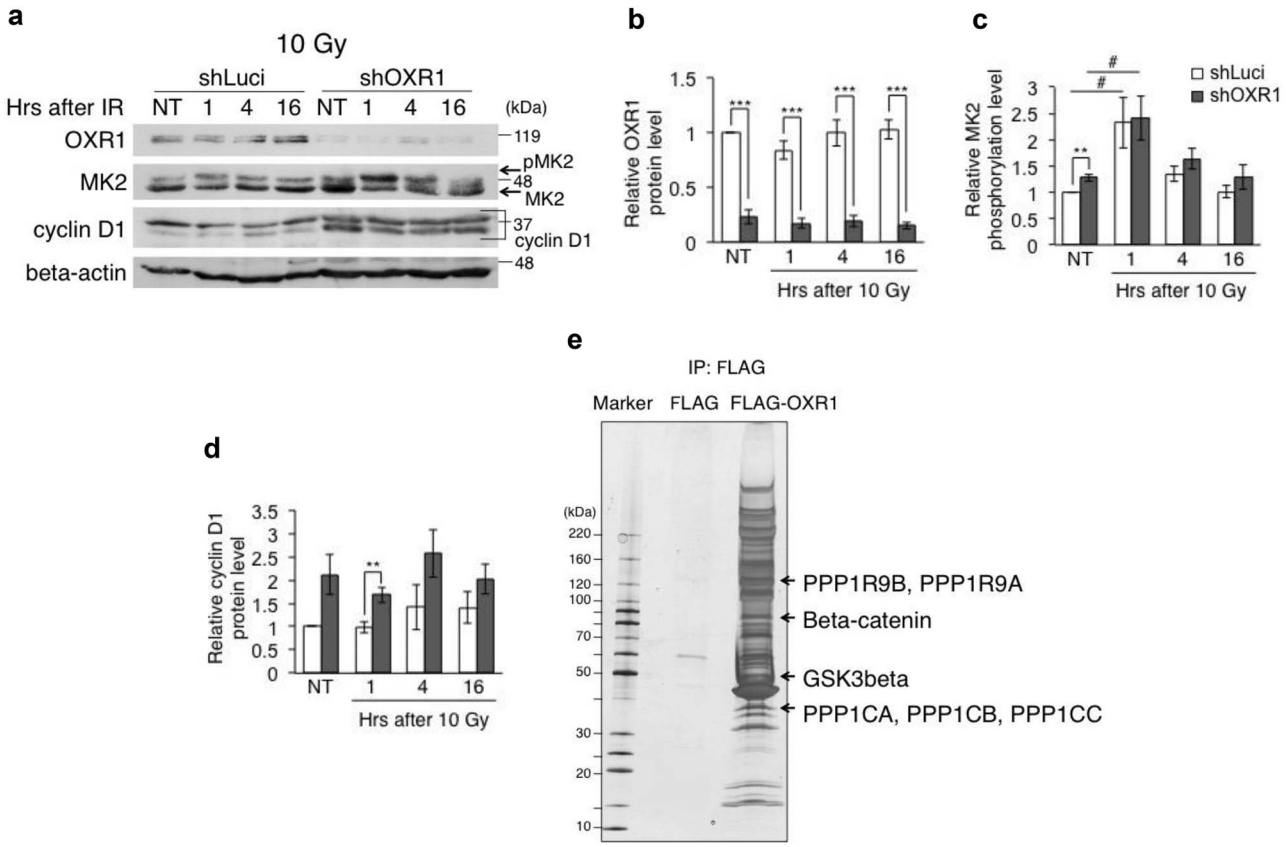

Fig. 4. OXR1-depletion affects the state of the cell cycle regulator. (a–d) Quantification of the level of MK2 phosphorylation and cyclin D1 expression after irradiation with 10 Gy of γ-rays. (a) Representative western blot for graphs b–d. (b–d) The images of western blot were analyzed by ImageJ software. Mean ± s.e.m. of *n* = five independent experiments, $^{\#}P < 0.05$, two-way ANOVA with Dunnett's multiple comparisons test, $^{**}P < 0.01$, $^{***}P < 0.001$, two-tailed Welch's t-test and Student's t-test. NT, non-irradiation. The anti-MK2 antibody detects two bands: the upper band is phosphorylated MK2 (pMK2) and the lower band is dephosphorylated MK2 (MK2) [44]. (e) Identification of OXR1-binding proteins. The empty vector plasmid (FLAG) or FLAG-OXR1-expressing vector plasmid (FLAG-OXR1) was transfected to Flp-In T-REx HEK293 cells. Proteins that bound specifically to FLAG-OXR1 were obtained using anti-Flag antibody and separated by SDS-PAGE. These proteins were identified by LC/MS/MS. IP, immunoprecipitation.

maintained [18]. G2/M arrest is induced in OXR1-depleted cells. However, the duration of it is shortened (Fig. 3a). These results suggest that OXR1 regulates maintenance of G2/M arrest. It has been reported that MK2 or cyclin D1 affects the duration of G2/M arrest [43, 44, 47]. OXR1-depletion did not impair the increase in MK2 phosphorylation in response to irradiation (Fig. 4c), whereas OXR1-depletion increased the level of cyclin D1 expression after irradiation (Fig. 4d). OXR1 probably binds to GSK3beta, an inhibitor of cyclin D1 expression directly and indirectly via interaction with cyclin D1 protein, or beta-catenin, a transcription factor [49, 50], supporting the idea that OXR1 contributes to regulation of cyclin D1 protein expression (Supplementary Fig. S6, see online supplementary material). Therefore, it is possible that OXR1 maintains the duration of G2/M arrest through regulation of cyclin D1 expression.

OXR1-depletion increased cellular sensitivity to 0.25 mM H_2O_2 (Supplementary Fig. S1e, see online supplementary material), whereas it had no effect on it following γ-ray irradiation (Fig. 1b). The abrogation of the G2 checkpoint is thought to lead to radioresistance [54]. OXR1-depletion-induced sensitivity to oxidative stress can be abolished by radioresistance. It is also possible that the concentration of γ-ray-generated H_2O_2 is too low to cause the consequence of cell lethality. The concentration of H_2O_2 in cells irradiated with ∼1 Gy/min of γ-rays is estimated to be in the nanomolar to micromolar range [55–58]. This value is much lower than that in cells treated with 0.25 mM H_2O_2 [59]. OXR1-depleted cells were not highly sensitive to superoxide generator (Supplementary Fig. S1f). To clarify how OXR1 contributes to cellular survival, further investigation is underway in our laboratory.

In this study, we present evidence that OXR1 protects genome stability against oxidative stress (Fig. 5). This effect may be derived from inhibition of the increase in superoxide level. In addition, OXR1 contributes to maintenance of the duration of G2/M arrest to defend

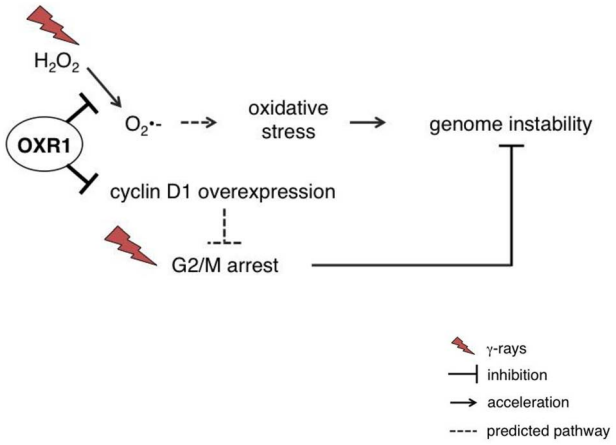

Fig. 5. Schematic view of OXR1 functions to prevent genome instability. OXR1 maintains the duration of G2/M arrest and inhibits elevation of the oxidative stress level in cells exposed to H_2O_2 or γ-rays. Through these two pathways, OXR1 protects nuclear genome stability under stress conditions.

genome stability. This may be caused by regulation of cyclin D1 expression. Further study is underway to confirm the interaction of OXR1 with cell cycle regulators in our laboratory.

CONCLUSION

This study demonstrates that OXR1 contributes to maintenance of genome stability by cell cycle regulation as well as oxidative stress inhibition.

SUPPLEMENTARY DATA

Supplementary data are available at *RADRES* online.

ACKNOWLEDGEMENTS

We thank Mr. Osamu Takahashi (KEYENCE) for observation of the hyper-plasmid transfected cells. We also thank Mr. Masafumi Funakoshi for critical reading of this manuscript.

CONFLICT OF INTEREST

The authors declare no competing financial interests.

FUNDING

Irradiation experiments were performed at the Joint Usage/Research Center at the Radiation Biology Center, Kyoto University. This work was supported by the Cooperative Research Project program of the Joint Usage/Research Center at the Institute of Development, Aging and Cancer, Tohoku University [2016–2 to A.M. and 2018–46 to Q.Z.A.]. This work was supported in part by Grants-in-Aid for Scientific Research from the Ministry of Education, Culture, Sports, Science and Technology of Japan [16 K00545 to Q.Z.A].

AUTHORS' CONTRIBUTIONS

A.M. and Q.Z.A. designed the project. A.M. designed the experiments. A.M., J.K., K.H., S.K. and A.Y. performed the experiments. A.M., M.M., Y.Y., S.K. and A.Y. analyzed the data. A.M., M.M. and Y.Y. wrote the manuscript. All authors commented on and approved the manuscript.

REFERENCES

1. Sies H, Berndt C, Jones DP. Oxidative stress. *Annu Rev Biochem* 2017;86:715–48.
2. Ciccia A, Elledge SJ. The DNA damage response: Making it safe to play with knives. *Mol Cell* 2010;40:179–204.
3. Sanada Y, Asai S, Ikemoto A et al. Oxidation resistance 1 is essential for protection against oxidative stress and participates in the regulation of aging in Caenorhabditis elegans. *Free Radic Res* 2014;48:919–28.
4. Oliver PL, Finelli MJ, Edwards B et al. Oxr1 is essential for protection against oxidative stress- induced Neurodegeneration. *PLoS Genet* 2011;7. doi: 10.1371/journal.pgen.1002338.
5. Liu KX, Edwards B, Lee S et al. Neuron-specific antioxidant OXR1 extends survival of a mouse model of amyotrophic lateral sclerosis. *BRAIN* 2015;138:1167–81.
6. Li Y, Li W, Liu C et al. Delivering oxidation Resistance-1 (OXR1) to mouse kidney by genetic modified Mesenchymal stem cells exhibited enhanced protection against nephrotoxic serum induced renal injury and lupus nephritis. *J Stem Cell Res Ther* 2014;4:231.
7. Volkert MR, Elliott NA, Housman DE. Functional genomics reveals a family of eukaryotic oxidation protection genes. *Proc Natl Acad Sci U S A* 2000;97:14530–5.
8. Elliott NA, Volkert MR. Stress induction and mitochondrial localization of Oxr1 proteins in yeast and humans. *Mol Cell Biol* 2004;24:3180–7.
9. Jaramillo-Gutierrez G, Molina-Cruz A, Kumar S et al. The Anopheles gambiae oxidation resistance 1 (OXR1) gene regulates expression of enzymes that detoxify reactive oxygen species. *PLoS One* 2010;5:e11168.
10. Kobayashi N, Takahashi M, Kihara S et al. Cloning of cDNA encoding a Bombyx mori homolog of human oxidation resistance 1 (OXR1) protein from diapause eggs, and analyses of its expression and function. *J Insect Physiol* 2014;68:58–68.
11. Yang M, Luna L, Sørbø JG et al. Human OXR1 maintains mitochondrial DNA integrity and counteracts hydrogen peroxide-induced oxidative stress by regulating antioxidant pathways involving p21. *Free Radic Biol Med* 2014;77:41–8.
12. Yang M, Lin X, Rowe A et al. Transcriptome analysis of human OXR1 depleted cells reveals its role in regulating the p53 signaling pathway. *Sci Rep* 2015;5:1–12.
13. Finelli MJ, Sanchez-Pulido L, Liu KX et al. The evolutionarily conserved Tre2/Bub2/Cdc16 (TBC), lysin motif (LysM), domain catalytic (TLDc) domain is neuroprotective against oxidative stress. *J Biol Chem* 2016;291:2751–63.
14. Wu Y, Davies KE, Oliver PL. The antioxidant protein Oxr1 influences aspects of mitochondrial morphology. *Free Radic Biol Med* 2016;95:255–67.
15. Zhang X, Zhang S, Liu X et al. Oxidation resistance 1 is a novel senolytic target. *Aging Cell* 2018. doi: 10.1111/acel.12780.

16. Murphy KC, Volkert MR. Structural/functional analysis of the human OXR1 protein: Identification of exon 8 as the anti-oxidant encoding function. *BMC Mol Biol* 2012;13:26.
17. Su LD, Zhang QL, Lu ZQ. Oxidation resistance 1 (OXR1) participates in silkworm defense against bacterial infection through the JNK pathway. *Insect Science.* 2017;24:17–26.
18. Kousholt AN, Menzel T, Storgaard SC. Pathways for genome integrity in G2 phase of the cell cycle. *Biomolecules* 2012;2:579–607.
19. Feinendegen LE. Reactive oxygen species in cell responses to toxic agents. *Hum Exp Toxicol* 2002;21:85–90.
20. Hong Z, Jiang J, Lan L et al. A polycomb group protein, PHF1, is involved in the response to DNA double-strand breaks in human cell. *Nucleic Acids Res* 2008;36:2939–47.
21. Enzo Life Sciences. Product manual: ROS-ID® Total ROS/superoxide detection kit. 2016.
22. BD Biosciences. BD FACSCalibur Instructions For Use. IN: 2007.
23. Schindelin J, Arganda-Carreras I, Frise E et al. Fiji: An open-source platform for biological-image analysis. *Nat Methods* 2012;9: 676.
24. Homma Y, Kanno SI, Sasaki K et al. Insulin receptor substrate-4 binds to slingshot-1 phosphatase and promotes cofilin dephosphorylation. *J Biol Chem* 2014;289: 26302–13.
25. O'Malley YQ, Reszka KJ, Spitz DR et al. Pseudomonas aeruginosa pyocyanin directly oxidizes glutathione and decreases its levels in airway epithelial cells. *Am J Physiol Cell Mol Physiol* 2004;287:L94–103.
26. Belousov VV, Fradkov AF, Lukyanov KA et al. Genetically encoded fluorescent indicator for intracellular hydrogen peroxide. *Nat Methods* 2006;3:281–6.
27. Ying W. NAD^+/NADH and $NADP^+$/NADPH in cellular functions and cell death: Regulation and biological consequences. *Antioxid Redox Signal* 2008;10:179–206.
28. Flora SJS. Arsenic-induced oxidative stress and its reversibility. *Free Radic Biol Med* 2011;51:257–81.
29. Orr AL, Kim C, Jimenez-Morales D et al. Neuronal Apolipoprotein E4 expression results in proteome-wide alterations and compromises bioenergetic capacity by disrupting mitochondrial function. *J Alzheimer's Dis* 2019;68:991–1011.
30. Yamamori T, Yasui H, Yamazumi M et al. Ionizing radiation induces mitochondrial reactive oxygen species production accompanied by upregulation of mitochondrial electron transport chain function and mitochondrial content under control of the cell cycle checkpoint. *Free Radic Biol Med* 2012;53: 260–70.
31. Liu R, Fan M, Candas D et al. CDK1-mediated SIRT3 activation enhances mitochondrial function and tumor Radioresistance. *Mol Cancer Ther* 2015;14:2090–102.
32. Fenech M, Kirsch-Volders M, Natarajan AT et al. Molecular mechanisms of micronucleus, nucleoplasmic bridge and nuclear bud formation in mammalian and human cells. *Mutagenesis* 2011;26:125–32.
33. Aruoma OI, Halliwell B, Hoey BM et al. The antioxidant action of N-acetylcysteine: Its reaction with hydrogen peroxide, hydroxyl radical, superoxide, and hypochlorous acid. *Free Radic Biol Med* 1989;6:593–7.
34. Benrahmoune M, Thérond P, Abedinzadeh Z. The reaction of superoxide radical with N-acetylcysteine. *Free Radic Biol Med* 2000;29:775–82.
35. Saenko Y, Cieslar-Pobuda A, Skonieczna M et al. Changes of reactive oxygen and nitrogen species and mitochondrial functioning in human K562 and HL60 cells exposed to ionizing radiation. *Radiat Res* 2013;180:360–6.
36. Yamamoto K, Ikenaka Y, Ichise T et al. Evaluation of mitochondrial redox status and energy metabolism of X-irradiated HeLa cells by LC/UV, LC/MS/MS and ESR. *Free Radic Res* 2018;52:648–60.
37. Yoshikawa Y, Yamasaki A, Takatori K et al. Excess processing of oxidative damaged bases causes hypersensitivity to oxidative stress and low dose rate irradiation. *Free Radic Res* 2015;49:1239–48.
38. Wojewódzka M, Buraczewska I, Kruszewski M. A modified neutral comet assay: Elimination of lysis at high temperature and validation of the assay with anti-single-stranded DNA antibody. *Mutat Res - Genet Toxicol Environ Mutagen* 2002;518: 9–20.
39. Lewis CW, Golsteyn RM. Cancer cells that survive checkpoint adaptation contain micronuclei that harbor damaged DNA. *Cell Cycle* 2016;15:3131–45.
40. Forment JV, Kaidi A, Jackson SP. Chromothripsis and cancer: Causes and consequences of chromosome shattering. *Nat Rev Cancer* 2012;12:663–70.
41. Sarkaria JN, Busby EC, Tibbetts RS et al. Inhibition of ATM and ATR kinase activities by the radiosensitizing agent, caffeine. *Cancer Res* 1999;59:4375–82.
42. Yan Y, Black CP, Cowan KH. Irradiation-induced G2/M checkpoint response requires ERK1/2 activation. *Oncogene* 2007;26:4689–98.
43. Reinhardt HC, Aslanian AS, Lees JA et al. p53-deficient cells rely on ATM- and ATR-mediated checkpoint Signaling through the p38MAPK/MK2 pathway for survival after DNA damage. *Cancer Cell* 2007;11:175–89.
44. Reinhardt HC, Hasskamp P, Schmedding I et al. DNA damage activates a spatially distinct late cytoplasmic cell-cycle checkpoint network controlled by MK2-mediated RNA stabilization. *Mol Cell* 2010;40:34–49.
45. Bertoli C, Skotheim JM, de Bruin RAM. Control of cell cycle transcription during G1 and S phases. *Nat Rev Mol Cell Biol* 2013;14:518–28.
46. Baldin V, Lukas J, Marcote MJ et al. Cyclin D 1 is a nuclear protein required for cell cycle progression in G1. *Genes Dev* 1993;7:812–21.
47. Martin JMC, Balkenende A, Verschoor T et al. Cyclin D1 overexpression enhances radiation-induced apoptosis and Radiosensitivity in a breast tumor cell line. *Cancer Res* 1999;59: 1134–40.
48. Zou Y, Ewton DZ, Deng X et al. Mirk/dyrk1B kinase destabilizes cyclin D1 by phosphorylation at threonine 288. *J Biol Chem* 2004;279:27790–8.

49. Takahashi-Yanaga F, Sasaguri T. GSK-3β regulates cyclin D1 expression: A new target for chemotherapy. *Cell Signal* 2008;20:581–9.
50. Diehl JA, Cheng M, Roussel MF et al. Glycogen synthase kinase-3β regulates cyclin D1 proteolysis and subcellular localization. *Genes Dev* 1998;12:3499–511.
51. Shi Y. Serine/threonine phosphatases: Mechanism through structure. *Cell* 2009;139:468–84.
52. Szatmari E, Habas A, Yang P et al. A positive feedback loop between glycogen synthase kinase 3β and protein phosphatase 1 after stimulation of NR2B NMDA receptors in forebrain neurons. *J Biol Chem* 2005;280:37526–35.
53. Sabharwal SS, Schumacker PT. Mitochondrial ROS in cancer: Initiators, amplifiers or an Achilles' heel? *Nat Rev Cancer* 2014;14:709–21.
54. Syljuasen RG, Jensen S, Bartek J et al. Adaptation to the ionizing radiation-induced G2 checkpoint occurs in human cells and depends on checkpoint kinase 1 and polo-like kinase 1 kinases. *Cancer Res* 2006;66:10253–7.
55. Meesungnoen J, Benrahmoune M, Filali-Mouhim A et al. Monte Carlo calculation of the primary radical and molecular yields of liquid water radiolysis in the linear energy transfer range 0.3-6.5 keV/micrometer: Application to 137Cs gamma rays. *Radiat Res* 2001;155:269–78.
56. Matsumoto K, Nyui M, Ueno M et al. A quantitative analysis of carbon-ion beam-induced reactive oxygen species and redox reactions. *J Clin Biochem Nutr* 2019;65:1–7.
57. Yamaguchi T, Muraiso C, Furuno-Fukushi I et al. Water content in cultured mammalian cells for Dosimetry of Beta-rays from Tritiated water. *J Radiat Res* 1990;31: 333–9.
58. Ameziane-El-Hassani R, Boufraqech M, Lagente-Chevallier O et al. Role of H_2O_2 in RET/PTC1 chromosomal rearrangement produced by ionizing radiation in human thyroid cells. *Cancer Res* 2010;70:4123–32.
59. Sies H. Hydrogen peroxide as a central redox signaling molecule in physiological oxidative stress: Oxidative eustress. *Redox Biol* 2017;11:613–9.